Interference structures in photoelectron spectra of atoms ionized by XUV pulses in the presence of a strong IR field

Ji-Wei Geng, Liang-You Peng,* Shu-Na Song, and Qihuang Gong
State Key Laboratory for Mesoscopic Physics and Department of Physics, Peking University, Beijing 100871, China
(Received 26 September 2013; published 18 November 2013)

The dynamics of photoelectrons ionized by XUV pulses in the presence of a strong infrared (IR) field is theoretically investigated by solving the time-dependent Schrödinger equation (TDSE). We study the ionization dynamics of He by an XUV pulse in the presence of a relatively strong IR laser field, which is different from the conventional attosecond streaking experiments where a rather weak IR field is applied. Comparing with the photoelectron spectra produced by the IR field only, we find the spectra ionized by the combined fields construct interesting interference structures for different XUV photon energies and pulse intensities. These features can be analyzed and explained by a quantum-trajectory theory based on the strong-field approximation (SFA). The SFA theory shows excellent agreement with the TDSE results, revealing that these structures originate from interferences among photoelectrons ionized by XUV pluses (streaked by the strong IR field) at different moments, and in some energy regions, together with the photoelectrons ionized by the intense IR pulse itself.

DOI: 10.1103/PhysRevA.88.053418 PACS number(s): 32.80.Rm, 34.50.Rk, 42.50.Hz

I. INTRODUCTION

The generation of attosecond pulses [1,2] has opened a new way to investigate the basic dynamics of atoms and molecules on their natural time scale. Attosecond streaking experiments, where attosecond XUV pulses are synchronized to an IR pulse, have been used to characterize both the attosecond pulse and the IR field [3–5]. More importantly, this technique has been applied to trace and control the electronic motion inside atoms and molecules. For example, attosecond streaking has been used to study the transient absorption of laser-dressed atoms both experimentally and theoretically [6–9], and to characterize the photoionization time- delays in atoms [10,11]. The basic idea of attosecond streaking experiments is based on a variant of a pump-probe setting with an attosecond pulse as a pump and a phase-controlled few-cycle infrared (IR) pulse as a probe. Photoelectrons pumped into the continuum by attosecond pulses are then accelerated by the electric field of the IR field to different final energies, depending on the value of the vector potential at the electron release time [3,12]. In the above attosecond streaking experiments, the intensity of the IR field usually used is relatively low, which only causes a momentum shift in the momentum spectra along the laser polarization direction, avoiding the pollution of the ionization signals induced by the IR field.

For a moderately stronger IR field, the electronic wave packets (EWPs) created by XUV attosecond pulses can be controlled by the IR field. At a later time of its birth, part of the EWPs can be driven back to collide with the ionic core. However, the IR laser field needed to drive the low-energy EWPs back to the core is still not strong enough to cause significant direct ionization. In the above situation, the creation and acceleration of the EWPs are decoupled, which is difficult to achieve by using a single strong IR pulse where the same pulse governs both events. Interference peaks separated by one-photon energy of the IR field has been observed in the low-energy region of the photoelectron spectra [13], which is beyond the description of the strong field approximation. It was demonstrated that interferences result from multiple collisions of the XUV-ionized EWPs driven by the IR field. In the case of attosecond pulse trains, laser-induced coherent electron scattering was experimentally observed in the electron momentum spectra [14]. In our previous work [15,16], we considered the dynamics of atoms ionized by a single attosecond pulse combined with a moderately strong IR field. We found interference structures appearing at the low-energy part of the photoelectron energy spectra, which was analyzed by a semiclassical method. We suggested that this laser-induced low-energy attosecond streaking promises a holographic imaging of atomic and molecular potential by the EWPs, in which the target potential is "scanned" by the rescattered electrons and the directly ionized electrons serve as a "reference" beam.

In past few years, several important free electron laser (FEL) facilities in the world have been able to generate XUV pulses with variable durations in femtoseconds scale [17–19]. When applied to atoms or molecules, these new light sources may produce significant amount of photoelectrons. Therefore, it would be interesting to study the ionization dynamics in the combined fields of such XUV pulses or attosecond pulses in the presence of a relatively stronger IR pulse. In this case, the IR pulse alone may produce significant ionization, which is different from situations discussed in previous paragraphs. Under the interaction of XUV pulses combined with an IR field at even higher intensities, many new phenomena are still unveiled. Recently, the dynamics of the laser-driven electron recollision wave packet was investigated by using a strong IR pulse combined with attosecond pulses [20]. When the recolliding electrons of the IR field revisit the parent ion, they can absorb an XUV photon, yielding high-energy electrons. By changing the time delay between the driving IR laser and the attosecond pluse, the recollision energy of the electrons can be retrieved. In the present paper, we focus on the interference structures in photoelectron energy spectra ionized by strong IR fields combined with XUV pulses. By changing the time delay between the two pulses, the duration and photon energy of the XUV pulse, we find the physical origin of the interference

*liangyou.peng@pku.edu.cn

structures in the energy spectra. Finally, trajectory-based strong-field approximation [21–23] is used to clearly show the physical insight of these processes.

The rest of the paper is organized as follows. In Sec. II, we briefly describe our theoretical method, which is based on the *ab initio* solution of the time-dependent Schrödinger equation. In Sec. III, we present our numerical results and discuss the physical mechanism of the interference structures in the electron energy spectra and carry out strong field approximation analysis. Finally, we make a short discussion and conclusion in Sec. IV.

II. THEORETICAL METHOD

Our theoretical approach is based on our previous work on the direct solution of the full-dimensional, time-dependent Schrödinger equation (TDSE) for a single-electron atom in the presence of a strong laser pulse [15,16,24]. In the present work, we consider the He atom under the joint interaction of an XUV pulse and an intense IR laser pulse, with both pulses assumed to be linearly polarized. For the He atom, we employ the effective one-electron potential given by Hartree [25], which reproduces the He ionization potential to an accuracy of 10^{-3}.

The TDSE of He interacting with a linearly polarized laser field is given by

$$i\frac{\partial}{\partial t}\psi(\mathbf{r},t) = \left[-\frac{1}{2}\nabla^2 + V(r) + H_{\rm I}(t)\right]\psi(\mathbf{r},t), \qquad (1)$$

where $H_{\rm I}(t)$ is the interaction term of the active electron with the laser pulses. We solve Eq. (1) in both the velocity gauge $[\mathbf{p}\cdot\mathbf{A}(t)]$ and length gauge $[\mathbf{r}\cdot\mathbf{E}(t)\,]$ to check consistency of the results. We find that both gauges give essentially identical results. The total vector potential is given by $\mathbf{A}(t) = \mathbf{A}_{\rm ir}(t) + \mathbf{A}_{\rm XUV}(t)$, and the corresponding electric field $\mathbf{E}(t)$ given by $\mathbf{E}(t) = -\partial\mathbf{A}(t)/\partial t$.

In spherical coordinates, the angular part of the wave function is expanded in spherical harmonics and the corresponding partial wave radial part is discretized by the finite difference method. After the end of the laser pulses, the probability of a photoelectron with an asymptotic momentum $\mathbf{k}$ can then be obtained by a projection of the final wave function onto the scattering states of the field-free Hamiltonian, i.e.,

$$P(\mathbf{k}) = P(k,\theta,\varphi) = |\langle\Psi_{\mathbf{k}}^{-}(\mathbf{r})|\Psi(\mathbf{r},t_f)\rangle|^2. \qquad (2)$$

For a linearly polarized pulse, $P(\mathbf{k})$ has an azimuthal symmetry about φ. The corresponding azimuthal angle integrated differential ionization probability is given by

$$P(E,\theta) = 2\pi\sqrt{2E}\,P(k,\theta,\varphi=0), \qquad (3)$$

where E is the electron energy.

In the present work, the vector potentials of the IR field and the XUV pulse, both linearly polarized along z axis, are assumed to have a sin-square envelope, i.e.,

$$\mathbf{A}_{\rm ir}(t) = \mathrm{A}_{0,\rm ir}\sin^2\left(\frac{\pi t}{\tau_{\rm ir}}\right)\sin(\omega_{\rm ir}t + \varphi_{\rm ir}), \qquad (4)$$

$$\mathbf{A}_{\rm XUV}(t) = \mathrm{A}_{0,\rm XUV}\sin^2\left(\frac{\pi t}{\tau_{\rm XUV}}\right)\sin(\omega_{\rm XUV}t + \varphi_{\rm XUV}). \qquad (5)$$

In the following calculations, the parameters of the IR pulse are kept fixed: We choose a four-cycle IR laser pulse with a peak intensity of 5×10^{14} W/cm^2. At this intensity, the IR laser field alone can cause significantly ionization of the target atom, which makes the situation very different from the usual attosecond streaking experiment. In the following, by changing the parameters of the XUV pulse, such as the pulse duration, frequency, and the time delay between the two pulses, we explore the physical origin of the observed interference structures in energy spectra in detail.

III. NUMERICAL RESULTS AND DISCUSSION

In this section, we will present our main results. In Sec. III A, we introduce the remarkable enhancement region in the photoelectron energy spectra by using a long XUV pulse combined with a strong IR field. Note that, for our purpose in the present work, we only consider the differential ionization yield of the photoelectrons for $\theta = 0$ along the laser polarization direction, i.e., $P(E,\theta = 0)$.

By changing the duration of the XUV pulse and time delay between the two pulses, we find that the enhancement region in photoelectron energy spectra are mainly caused by two types of time delays. In Sec. III B, for the two types of time delays, we investigate the dependence of the enhancement region on different XUV intensities and photon energies, respectively. We conclude that the electron ionized by one-photon XUV absorbtion streaked by the IR laser field mainly contribute to the enhancement region. In some energy regions, the yield of photoelectrons ionized by the IR field itself is comparable with that of these streaked electrons and they will add up additional interference structures. Finally, in Sec. III C, by performing strong field approximation (SFA) analysis of these processes, we get a clear physical insight into the interference structures in the enhancement region in photoelectron energy spectra.

A. The enhancement region in photoelectron energy spectra

First, in the presence of the strong IR field, we use a long XUV pulse, which contains 100 cycles with peak intensity of $I_{\rm XUV} = 1\times10^{11}$ W/cm^2 at photon energy $\omega_{\rm XUV} = 1.5$ a.u. In Fig. 1(a), we show the electric fields of the combined laser pulses on the left panel and the corresponding differential photoelectron energy spectra for $\theta = 0$ on the right panel. We can clearly observe that, compared with the photoelectron energy spectra ionized by the IR field only, the combined fields cause a remarkable enhancement of the ionization yield in the energy region $2\sim6$ a.u. in the photoelectron energy spectra. This prominently yield-enhanced energy range is called as *an enhancement region* in the rest of the paper. One notices that the enhancement region consists of both large-scale interference peaks and finer interference structures.

In order to investigate how this enhancement region come into its formation, we put several XUV pulses with the same photon energy of 1.5 a.u. but with shorter pulse durations and different time delays with respect to the IR laser field. First, we put four three-cycle XUV pulses at the maxima of the IR electric field, respectively [Fig. 1(b)]. As can be seen from the right panel of Fig. 1(b), the resultant photoelectron distribution is very similar to the one produced by the IR

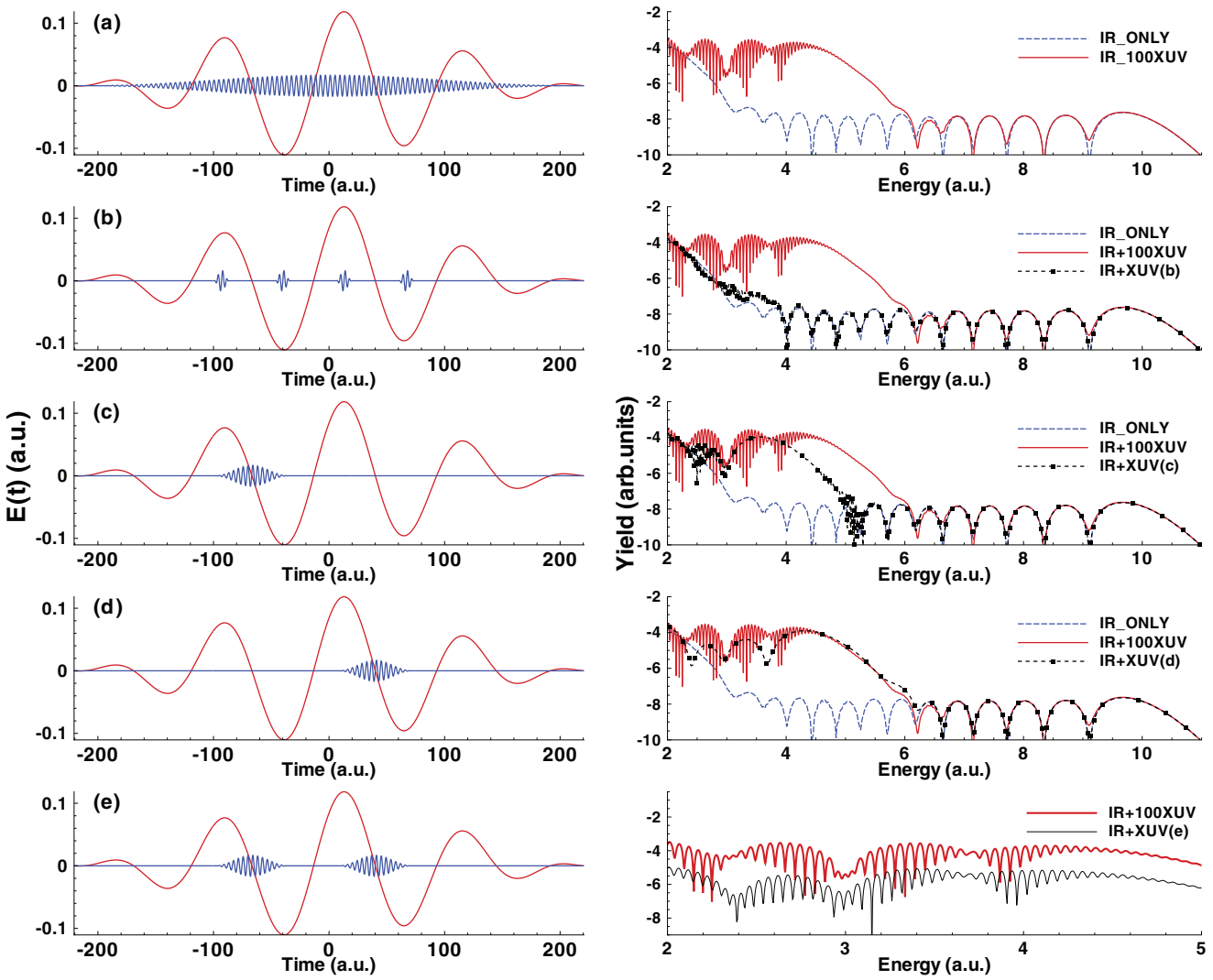

FIG. 1. (Color online) (Left column) The electric fields of the XUV pulse with photon energy $\omega_{\rm XUV} = 1.5$ a.u and peak intensity $I_{\rm XUV} = 1 \times 10^{11}$ W/cm^2, and of a four-cycle 800-nm IR pulse with $I_{\rm ir} = 5 \times 10^{14}$ W/cm^2. (Right column) The corresponding electron energy spectra for the pulse configuration shown in each row of the left column. In the right column of (a)–(d), the blue dashed line represents the photoelectron ionized by the IR field only and the red solid line is the energy spectra ionized by the combined field shown in (a) (i.e., a 100-cycle XUV pulse combined with the IR field). The black dash-squared line shows the electron spectra ionized by (b) four three-cycle XUV pulses positioned at the maxima of the electric field of IR pulse; (c) a 15-cycle XUV pulse with a time delay $t_1 = -67$ a.u.; (d) a 15-cycle XUV pulse with a time delay $t_2 = 40$ a.u. In (e), the upper red thick line represents the spectra for a 100-cycle XUV pulse combined with the IR field [shown in the right column of (a)]; the lower black thin line is the result for the case of two 15-cycle XUV pulses with a time delay of t_1 and t_2, respectively, which is shifted downwards for the clarity of the finer structures.

field alone, with only a little difference in the energy region of $2 \sim 6$ a.u. Secondly, we put a 15-cycle XUV pulse at the time delay $t_1 = -67$ a.u., which corresponds to the minimum of the IR laser field [Fig. 1(c)]. In this situation, the energy spectra formed by the combined field exhibits an enhancement region with a different large-scale structure and a lower cutoff energy, compared with those shown in the right panel of Fig. 1(a) for the case of the 100-cycle XUV pulse. When the same XUV pulse is shifted to a different time delay of $t_2 = 40$ a.u. in Fig. 1(d), one can observe an enhancement region, which almost has the same cutoff energy and the large-scale interference structures with those shown in Fig. 1(a), but with the absence of the finer interference structures. Finally, if one puts two 15-cycle XUV pulses at time delay t_1 and t_2, respectively [Fig. 1(e)], we can almost reproduce the same enhancement region with both large-scale and finer-scale structures, as those shown in Fig. 1(a) for the case of the 100-cycle XUV pulse.

From the above observations, one can conclude that the enhancement region is mainly caused by the interferences of the electrons when two XUV pulses are centered at time delay t_1 and t_2, respectively. The large scale interferences are caused by the attosecond ionization by one pulse but streaked by the IR pulse at different moments. The finer structures, roughly spaced with one IR photon energy, are formed by the interferences between the electrons ionized at t_1 and t_2, or in some energy regions, together with the photoelectrons ionized by the IR itself. In the next subsection,

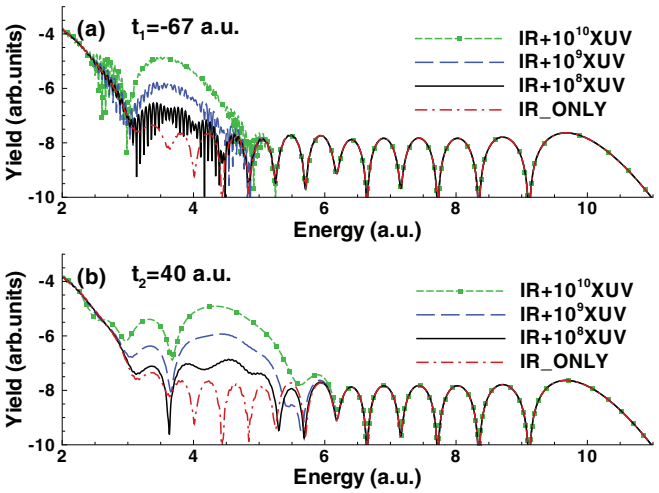

FIG. 2. (Color online) Comparisons of photoelectron spectra for different XUV intensities at the same XUV photon energy of 1.5 a.u. with a time delay of $t_1 = -67$ a.u. in (a) [cf. Fig. 1(c)] and $t_2 = 40$ a.u. in (b) [cf. Fig. 1(d)]. In both (a) and (b), from top to bottom is the spectra for the XUV pulse with peak intensity: 1×10^{10} W/cm^2 (green dash-squared), 1×10^9 W/cm^2 (blue long-dashed), 1×10^8 W/cm^2 (black solid), and the spectra ionized by the IR field only (red dash-dotted).

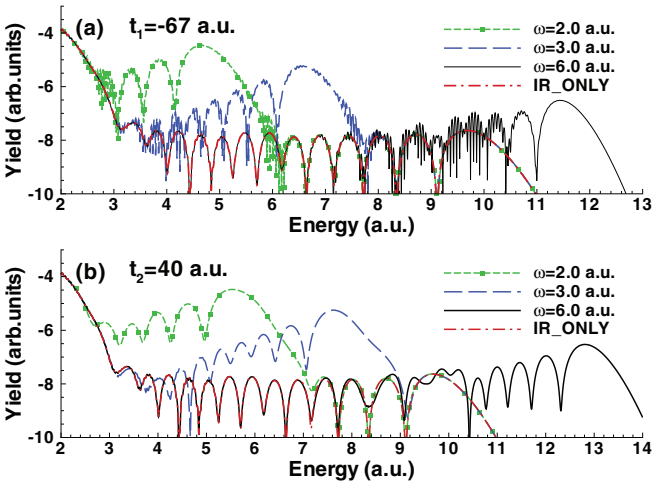

FIG. 3. (Color online) Comparisons of photoelectron spectra for different XUV photon energies at the same XUV intensity of 1×10^{11} W/cm^2 with a time delay of $t_1 = -67$ a.u. in (a) [cf. Fig. 1(c)] and $t_2 = 40$ a.u. in (b) [cf. Fig. 1(d)]. In both (a) and (b), from top to bottom is the spectra for the XUV pulse with photon energy: $\omega_{\rm XUV} = 2.0$ a.u. (green dash-squared), $\omega_{\rm XUV} = 3.0$ a.u. (blue long-dashed), $\omega_{\rm XUV} = 6.0$ a.u. (black solid), and the spectra ionized by the IR field only (red dash-dotted).

we numerically investigate the mechanisms of the different interference structures for time delay t_1 and t_2, respectively, for different XUV pulses.

B. Dependence on XUV intensity and photon energy

Now, we perform a series of TDSE simulations for different XUV laser parameters to understand the physical origin of the interference structures for time delay t_1 and t_2, respectively. Here we focus on the dependence of the interference structures on XUV intensities and XUV photon energies. At first, we keep the duration of the XUV pulse (15-cycle) and the photon energy ($\omega_{\rm XUV} = 1.5$ a.u.) unchanged but alter the XUV intensity for the two time delays, respectively. From Figs. 2(a) and 2(b), we can see that the yield of the enhancement region decreases with the dropping of the XUV intensity. For both time delays, the yield in the enhanced region almost has a linear scale with the XUV intensity, which indicates that the enhancement region is mainly caused by one-photon ionization of the XUV pulse. Another interesting phenomenon one can observe is that, with the decreasing of the XUV intensity, the enhancement region shows a much clearer fine-scale interference structure, especially at the lowest XUV intensity of 1×10^8 W/cm^2. We note that when a lower XUV intensity is used, the yield of photoelectrons ionized by the one-photon XUV may be reduced to be comparable with that caused by the IR field only. The photoelectrons from the two processes can thus interfere effectively, leading to the obvious interference structures at lower XUV intensities.

Next, we investigate the dependence of the enhancement region on the XUV photon energy for the two different time delays. We keep the XUV pulses with the same intensity of 1×10^{11} W/cm^2, but change the XUV photon energy. As shown in Fig. 3, with the increase of the XUV photon energy, the general feature of the interference structures in the enhancement region keeps unchanged but with a broader energy range and a lower yield for both two time delays. For example, the enhancement region formed for the case of $\omega_{\rm XUV} = 6.0$ a.u. has a much broader cutoff energy, which exceeds the usual $10U_p$ cutoff by the IR field alone. In addition, the yield of this enhancement region almost has comparable amplitude with the high-energy above-threshold ionization photoelectrons induced by the IR field alone.

Combined with the investigations in the previous paragraphs, one can affirm that the enhancement region is indeed mainly contributed by one-photon ionization of the XUV pulse, since it is well known that the one-photon ionization cross section decreases with the increase of the photon energies in the range discussed above. In the conventional attosecond streaking experiments, the momenta of the high-energy photoelectrons pumped into the continuum by XUV pulses are shifted by the IR electric field, where the effect of the Coulomb potential can be neglected. According to the Newtonian equation of motion, i.e., $\partial \mathbf{p}(t)/\partial t = -\mathbf{E}_{\rm ir}(t)$, the photoelectron momentum at the detector is given by

$$\mathbf{p}(t_\infty) = \mathbf{p}_0 - \mathbf{A}_{\rm ir}(t_0), \tag{6}$$

where t_0 is the release time of the electron by the XUV photon. The above equation lies in the basis of the attosecond streaking experiments.

In our numerical experiments, the IR field itself will cause significant ionization, which is in some cases comparable with the probability ionized by the one-photon absorption by the XUV pulse. The latter EPWs can be streaked by the strong IR field and achieve a similar momentum shift to that in the convention attosecond streaking. To confirm this, we can use Eq. (6) to approximate the cutoff energy in the enhanced region. The highest energy of the streaked electron can be obtained when the XUV pulse is put at the minimum of the

IR electric field. Based on Eq. (6), the corresponding cutoff energy streaked by the IR field is given by

$$E_{\text{cutoff}} = \tfrac{1}{2} \times [\sqrt{2(\omega_{\text{XUV}} - I_p)} - A_{\text{ir}}(t_0)]^2. \quad (7)$$

With $\omega_{\text{XUV}} = 6.0$ a.u., we estimate these classical cutoff energies for the two time delays to be 11.7 a.u. and 13.1 a.u., respectively, which is in good agreement with the TDSE results. The agreement is also very excellent for other XUV photon energies which is sufficiently large so that the Coulomb potential effect can be neglected. The cutoff energy streaked by the IR field of time delay t_1 is smaller comparing with that of time delay t_2 simply because the vector potential of the IR field at t_1 is slightly lower than that at time delay t_2. The above analysis confirms that photoelectrons ionized by XUV one-photon absorbtion and subsequently streaked by the IR field contribute to the main structures in the enhancement region.

It is noteworthy that, for $\omega_{\text{XUV}} = 6.0$ a.u., different interference structures appear around the electron energy of 10 a.u., which is near the cutoff induced by the IR field alone. Actually, these structures have the same origins with those observed in Fig. 2(a) at lower XUV intensities. This is because, at these laser parameters, the probability of electrons induced by the IR field alone and that ionized by the XUV pulse are comparable in the energy regions discussed above. Therefore, the two processes can interfere effectively with each other to give additional interesting structures.

C. Strong field approximation analysis

According to the discussions in the previous subsections, the probability of an atom interacting with an XUV pulse combined with an IR laser field can be formulated by

$$P = |M_{\text{ir}} + M_{\text{XUV\_streaked}}|^2, \quad (8)$$

where M_{ir} and $M_{\text{XUV\_streaked}}$ is, respectively, the transition amplitude of the above-threshold ionization by the IR pulse alone and the XUV one-photon ionization streaked by the IR field. When these two transition amplitudes are comparable, they will interfere and lead to additional interference structures in the energy spectra. In order to give physical insight into the origin of the interference structures for the two different time delays, we perform strong field approximation (SFA) analysis of this process. SFA is a widely used theoretical tool in the field of strong field physics and has been applied to various nonperturbative ionization processes [26–28].

For the IR governed ionization in particular, SFA provides an intuitive semiclassical interpretation of strong field phenomena in terms of "quantum orbits." The transition amplitude of SFA from the initial state $|\psi_0(t)\rangle$ to the final Volkov state $|\psi_{\mathbf{p}}^V(t)\rangle$ reads

$$M_{\mathbf{p}}^{\text{SFA}} = M_{\mathbf{p}}^{(0)} + M_{\mathbf{p}}^{(1)}, \quad (9)$$

in which

$$M_{\mathbf{p}}^{(0)} = -i \int_0^T dt \langle \psi_{\mathbf{p}}^V | \mathbf{r} \cdot \mathbf{E}_{\text{ir}}(t) | \psi_0 \rangle, \quad (10)$$

$$M_{\mathbf{p}}^{(1)} = -\int_0^T dt \int_0^{t_1} \langle \psi_{\mathbf{p}}^V | V(\mathbf{r}) U_{\mathbf{k}} \mathbf{r} \cdot \mathbf{E}_{\text{ir}} | \psi_0 \rangle, \quad (11)$$

where $V(\mathbf{r})$ is a scattering potential of the Yukawa type and $U_{\mathbf{k}}$ is the Volkov time-evolution operator [28]. In the above equations, the transition amplitude $M_{\mathbf{p}}^{(0)}$ is the so-called Keldysh-Faisal-Reiss (KFR) amplitude [29–31] and accounts for the direct ionization, which implies an electron ionized into the continuum is driven towards the detector by the external laser fields without further interaction with the core. Because of neglecting the Coulomb potential, the transition amplitude $M_{\mathbf{p}}^{(0)}$ cannot even qualitatively match the experiment data and TDSE results. The transition amplitude $M_{\mathbf{p}}^{(1)}$ is the rescattering amplitude, which is responsible for the high-energy plateau in the electron energy spectra. $M_{\mathbf{p}}^{(1)}$ corresponds to the electrons after the rescattering with the core in the so-called three-step model [28,32]. In the high-energy plateau region, the prediction of $M_{\mathbf{p}}^{(1)}$ usually has a good qualitative agreement with the exact TDSE result except for the absolute ionization probability.

In the case of XUV photoionization in the presence of the strong IR field, SFA can also give a good description [12]. The reason is that the central frequency of the XUV pulse is usually much larger than the ionization potential, which ensures that the neglecting of the Coulomb potential is a reasonable assumption. Within this approximation, once the electron is ionized by the XUV pulse, its subsequent dynamics is solely governed by the IR field. So the final state can be approximated by the Volkov state. Therefore, the transition amplitude of the XUV one-photon ionization streaked by the IR field can be given by

$$M_{\text{XUV\_streaked}} = -i \int_{-\infty}^{\infty} dt \langle \psi_{\mathbf{p}}^V(t) | \mathbf{r} \cdot \mathbf{E}_{\text{XUV}}(t) | \psi_0(t) \rangle, \quad (12)$$

where $\mathbf{E}_{\text{XUV}}(t)$ is the electric field of the XUV pulse.

In the following, we use SFA to analyze the interference structures observed for the two time delays, respectively. We start our discussion for $\omega_{\text{XUV}} = 6.0$ a.u. In this case, the XUV photon energy is much larger than the ionization potential of ground-state He, enabling the SFA applicable. In addition, as seen in the previous subsection, the ionization by the XUV one-photon ionization has a comparable probability with that of the high-energy plateau formed by the direct IR field ionization through the rescattering process. The latter amplitude by the IR field can be easily calculated with an intuitive picture by a few quantum orbits based on the saddle-point method. The above condition ensures that SFA theory can give a good description of the problem. The saddle-point approximation [22,23] is used to carry out the integration for the transition amplitude $M_{\mathbf{p}}^{(1)}$. The five-dimensional integral over the intermediate electron momentum, the ionization time, and the rescattering time are approximated by the sum of contributions determined by the solutions to the saddle-point equations. The integration in the transition amplitude $M_{\mathbf{p}}^{(1)}$ is thus recast in the form of a sum over all relevant saddle points. Actually, for the parameters of the IR field we use, only four pairs of such solutions mainly contribute to the electron emission in the high-energy plateau. As shown in Fig. 4(a), solutions 1,2 and 3,4 correspond, respectively, to the long and short trajectory of the electrons ionized at the adjacent peak of the IR electric field. The electrons are rescattered almost at the same time, shown as a dashed curve in Fig. 4(a). These four trajectories

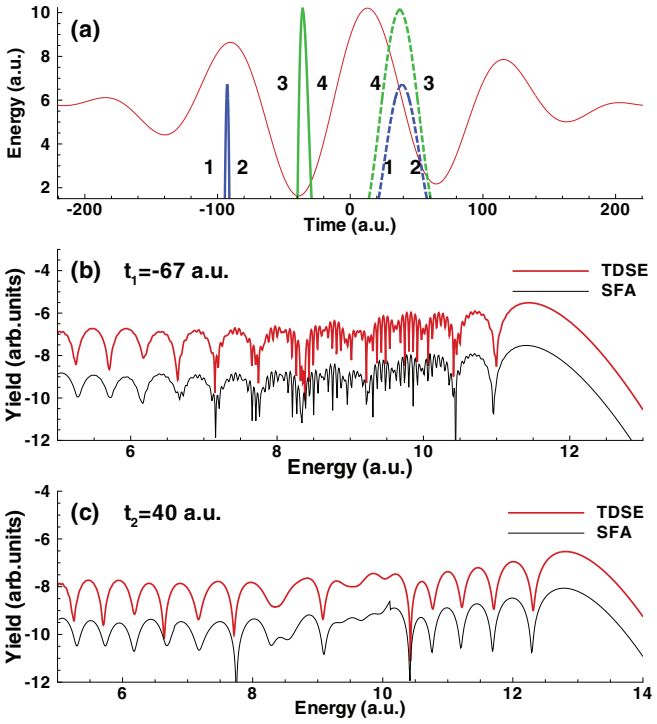

FIG. 4. (Color online) (a) The final electron energies as a function of the real part of the solutions to the saddle point equations for the ionization time (solid blue line for pairs 1, 2 and solid green line for pairs 3, 4), against the IR electric field (solid red curve). Also shown are the corresponding rescattering times (dashed lines). Only four pairs of solutions are presented here, which mostly contribute to the plateau region of the energy spectra for electron emission in the direction $p_z > 0$. (b) and (c) Comparisons of the energy spectra calculated by TDSE (red upper thick line) and the SFA (black lower thin line) for the time delay t_1 and t_2, respectively. The photon energy and intensity of the XUV pulse is taken to be $\omega_{\rm XUV} = 6.0$ a.u. and $I_{\rm XUV} = 1 \times 10^{11}$ W/cm^2.

are coherently superposed to form the high-energy plateau of the IR resacttered electrons. For the XUV ionization process, one simply needs to numerically calculate the time integral in transition amplitude $M_{\rm XUV\_streaked}$ in Eq. (12). We need to point out that SFA can not accurately give the absolute ionization probability because no proper consideration is taken into account for the Coulomb potential. Nevertheless, SFA can produce qualitatively correct results and give intuitive physical insights into the problem at hand. In practice, one needs to scale the absolute amplitude of the two processes in order to obtain a best agreement with the TDSE results.

Now let us look at the comparisons of SFA predictions with the TDSE results for both time delays t_1 [Fig. 4(b)] and t_2 [Fig. 4(c)]. Note that, for clarity, we have deliberately avoided the overlapping of the SFA and TDSE results by a vertical shift. As shown in these two figures, both results agree with each other very well (after a global scale of the SFA result). One notes that, for both time delays, large scale interference structures are observed in the energy spectra, which is related to the intracycle interference [33]. To be specific, the duration of the XUV pulse for $\omega_{\rm XUV} = 6.0$ a.u. contains 45 cycles, almost equal to the half cycle of the IR pulse. So all the photoelectrons ionized by this XUV pulse essentially have the same initial momentum. When the XUV pulse is put at the zero of the IR electric field, these electrons with the same energy are released to the continuum at two different moments with the same IR vector potential. Therefore, according to Eq. (6), they will be streaked by the IR field to the same final energy at the detector and interfere with each other. Because these two events happen within a time scale less than one optical cycle of the IR pulse, they will lead to large-scale interferences observed, which is very similar to the interference peaks observed at the high-energy plateau region formed by the IR field alone through the resacttering process corresponding to the long and short trajectory.

For time delay t_1 shown in Fig. 4(b), besides the intracycle interference discussed above, there exist finer interference structures in the energy range of $7 \sim 11$ a.u. These fine interferences are roughly spaced by one IR photon energy and are related to the intercycle interference. In addition, at this time delay, the electrons ionized by the IR pulse from the trajectory 3 and 4 have comparable probability with that of electrons from one XUV photon absorption and streaked by the IR field. The two ionization events, leading to the same final electron energies, have approximately a time delay of one IR optical cycle, which will form the intercycle interferences observed. Please note that trajectories 1 and 2 have a smaller cutoff energy and much lower ionization probability, compared with trajectories 3 and 4. Therefore, trajectories 3 and 4 dominate the energy range of $7 \sim 11$ a.u in the IR alone ionization. The agreement of the positions of the interference peaks of SFA and the TDSE result is excellent, which confirms the physical origins of the large-scale and finer scale interference structures we observe in the present work.

IV. DISCUSSIONS AND CONCLUSIONS

In summary, we have carried out theoretical studies on the interference structures observed in the photoelectron spectra of He atoms ionized by an XUV pulse in the presence of an intense IR field. An enhancement region as a common feature is identified for different XUV intensities and XUV photon energies. The strong field approximation is successfully applied to interpret the interference patterns obtained at different time delays. We have demonstrated that the interference patterns in the energy spectra are formed by the coherent superpositions of the XUV one-photon ionization streaked by the IR field at different moments, and in some energy regions, together with the above-threshold ionization by the intense IR pulse itself. The SFA theory perfectly reproduces the interference structures for reasonably larger XUV photon energies. At low XUV photon energies, where SFA fails, the discrepancies do exist primarily due to the neglect of the Coulomb potential, which is under further scrutiny. The features we discuss in the present work can be experimentally observed by using XUV sources from the FEL facility or tabletop attosecond pulses, combined with a strong few-cycle IR pulse.

In the present work, we have only discussed the energy spectra of the electrons ionized along $\theta = 0$. Of course, this kind of interference is actually present in a certain cone around the axis of $\theta = 0$, among the signals of the streaked attosecond ionization at different time. In some energy regions, if the ionization signal by the IR pulse alone is comparable with

these streaked signals, it will add up additional interference structures. However, in the other half sphere of emitted electrons around the direction of $\theta = \pi$, we do not observe aforementioned enhancement regions, mainly because the yield of above-threshold ionization by the intense IR pulse dominates in those regions.

We point out the observed phenomena in this regime of stronger IR intensities may find potential applications in attosecond sciences. For example, in a very recent paper by Liu and coworkers [34], they investigated the ionization dynamics for the case where an isolated attosecond pulse is combined with a strong IR field. In their work, they demonstrated the feasibility of characterizing the carrier envelope phase of the attosecond pulse by using the interferences of the electrons from the streaked attosecond ionization and from the above-threshold ionization by the intense IR pulse itself. Their proposal opens the door to a complete characterization of the attosecond wave form. Further investigations of attosecond streaking in the stronger IR field may lead to more new physics and additional applications.

ACKNOWLEDGMENTS

This work is supported by the 973 Program under Grant No. 2013CB922402, by National Natural Science Foundation of China under Grants No. 11322437, No. 11174016, No. 11121091, and by Program for New Century Excellent Talents in University (NCET). The computational results were obtained by using the computer cluster "MESO" in the State Key Laboratory for Mesoscopic Physics at Peking University.

[1] P. M. Paul, E. S. Toma, P. Breger, G. Mullot, F. Augeé, Ph. Balcou, H. G. Muller, and P. Agostini, Science **292**, 1689 (2001).
[2] M. Hentschel, R. Kienberger, Ch. Spielmann, G. A. Reider, N. Milosevic, T. Brabec, P. B. Corkum, U. Heinzmann, M. Drescher, and F. Krausz, Nature (London) **414**, 509 (2001).
[3] F. Quéré, J. Itatani, G. L. Yudin, and P. B. Corkum, Phys. Rev. Lett. **90**, 073902 (2003).
[4] R. Kienberger *et al*., Nature (London) **427**, 817 (2004).
[5] E. Goulielmakis *et al*., Science **305**, 1267 (2004).
[6] P. Johnsson, J. Mauritsson, T. Remetter, A. L'Huillier, and K. J. Schafer, Phys. Rev. Lett. **99**, 233001 (2007).
[7] T. E. Glover *et al*., Nat. Phys. **6**, 69 (2009).
[8] M. Wickenhauser, J. Burgdörfer, F. Krausz, and M. Drescher, Phys. Rev. Lett. **94**, 023002 (2005).
[9] C. Buth, R. Santra, and L. Young, Phys. Rev. Lett. **98**, 253001 (2007).
[10] M. Schultze *et al*., Science **328**, 1658 (2010).
[11] A. S. Kheifets and I. A. Ivanov, Phys. Rev. Lett. **105**, 233002 (2010).
[12] M. Kitzler, N. Milosevic, A. Scrinzi, and F. Krausz, and T. Brabec, Phys. Rev. Lett. **88**, 173904 (2002).
[13] A. K. Kazansky and N. M. Kabachnik, J. Phys. B **40**, 2163 (2007).
[14] J. Mauritsson, P. Johnsson, E. Mansten, M. Swoboda, T. Ruchon, A. L'Huillier, and K. J. Schafer, Phys. Rev. Lett. **100**, 073003 (2008).
[15] L.-Y. Peng, E. A. Pronin, and A. F. Starace, New J. Phys. **10**, 025030 (2008).
[16] M. H. Xu, L. Y. Peng, Z. Zhang, Q. Gong, X. M. Tong, E. A. Pronin, and A. F. Starace, Phys. Rev. Lett. **107**, 183001 (2011).
[17] W. Ackermann *et al*., Nat. Photonics **1**, 336 (2007).
[18] T. Shintake *et al*., Nat. Photonics **2**, 555 (2008).
[19] B. McNeil, Nat. Photonics **3**, 375 (2009).
[20] O. Smirnova, S. Patchkovskii, and M. Spanner, Phys. Rev. Lett. **98**, 123001 (2007).
[21] D. B. Milošević and W. Becker, Phys. Rev. A **66**, 063417 (2002).
[22] D. B. Milošević, G. G. Paulus, D. Bauer, and W. Becker, J. Phys. B **39**, R203 (2006).
[23] R. Kopold, W. Becker, and M. Kleber, Opt. Commun. **179**, 39 (2000).
[24] L.-Y. Peng and A. F. Starace, J. Chem. Phys. **125**, 154311 (2006).
[25] D. R. Hartree, *The Calculation of Atomic Structures* (Wiley, New York, 1957).
[26] P. Salières *et al*., Science **292**, 902 (2001).
[27] M. Lewenstein, Ph. Balcou, M. Yu. Ivanov, A. L'Huillier, and P. B. Corkum, Phys. Rev. A **49**, 2117 (1994).
[28] W. Becker, F. Grasbon, R. Kopold, D. B. Milošević, G. G. Paulus, and H. Walther, Adv. At. Mol. Opt. Phys. **48**, 35 (2002).
[29] L. V. Keldysh, Sov. Phys. JETP **20**, 1307 (1965).
[30] A. K. Kazansky, J. Phys. B **6**, L89 (1973).
[31] H. R. Reiss, Phys. Rev. A **22**, 1786 (1980).
[32] P. B. Corkum, Phys. Rev. Lett. **71**, 1994 (1993).
[33] D. G. Arbó, K. L. Ishikawa, K. Schiessl, E. Persson, and J. Burgdorfer, Phys. Rev. A **81**, 021403(R) (2010).
[34] C. Liu, M. Reduzzi, A. Trabattoni, A. Sunilkumar, A. Dubrouil, F. Calegari, M. Nisoli, and G. Sansone, Phys. Rev. Lett. **111**, 123901 (2013).